Exploration of Interfacial Conductivity and Magnetism in Manganite/Cuprate Heterostructures

Bo Du(杜波)[1,2,3,4], Gangfan Chen(陈钢帆)[1,2,3,4], Yichi Zhang(张一弛)[1,2,3,4], Guangyu Xi(席光煜)[1,2,3,4], Jingyi Shen(沈静怡)[1,2,3,4], Yiwei Gu(顾易炜)[2,3,4], Yuan Liu(刘源)[1], Tianshuang Ren(任天爽)[1], Chuanyu Shi(史传宇)[1], Yanwu Xie(谢燕武)[1], and Jie Wu(吴颉)[2,3,4*]

[1]*School of Physics, Zhejiang University, Hangzhou 310027, China*
[2]*Research Center for Industries of the Future, Westlake University, Hangzhou 310024, China*
[3]*Department of Physics, School of Science, Westlake University, Hangzhou 310024, China*
[4]*Key Laboratory for Quantum Materials of Zhejiang Province, School of Science, Westlake University, Hangzhou 310024, China*

(Received 10 November 2025; accepted manuscript online 4 January 2026)

Superconductivity emerging at the interface of heterostructures provides a unique platform to study and control superconductivity at the two-dimensional limit and offers a promising avenue for discovering new superconducting materials. By adjoining an undoped cuprate layer, such as La_2CuO_4 (LCO) and $SrCuO_2$ (SCO), with a hole-doped $La_{1-x}Sr_xMnO_3$ (LSMO) layer, we systematically investigate the conductivity and magnetism of manganite/cuprate heterostructures while varying the LSMO doping level from 0.33 to 0.80 to tune LSMO from a ferromagnetic metal to an antiferromagnetic insulator. Driven by the difference in work functions, charges are transferred from the LSMO layer to the cuprate layer, thereby giving rise to a conducting interfacial layer when the LSMO layer is heavily doped. No signature of interface superconductivity is observed in any of the synthesized heterostructures, a behavior likely attributable to spin-polarized charge transfer and the competition between superconductivity and magnetism. Our findings provide valuable insights into the mechanism of interface superconductivity as well as guidelines for the search for emergent interfacial effects.

DOI: 10.1088/0256-307X/43/2/020710 CSTR: 32039.14.0256-307X.43.2.020710

1. Introduction. Heterointerfaces, distinct from their parent compounds in composition, lattice structure, and electronic, orbital, and spin interactions, can host emergent phenomena confined to the interface. The discovery of superconductivity at such interfaces has created opportunities for uncovering new superconducting families and probing superconducting mechanisms in two dimensions. Reported material systems include (overdoped $La_{2-x}Sr_xCuO_4$)/La_2CuO_4 (LSCO/LCO),[1–4] (monolayer FeSe)/$SrTiO_3$,[5–7] and several insulator/insulator heterostructures, such as $LaAlO_3/SrTiO_3$,[8] $LaAlO_3/KTaO_3$ (111),[9] $LaAlO_3/KTaO_3$ (110),[10] $EuO/KTaO_3$,[11–13] and other $KTaO_3$-based interfaces.[9] Yet, despite the rapidly expanding material base, the universal principles underlying interface superconductivity remain unclear, and its discovery is largely trial-and-error and often a matter of luck.

Studies of LSCO/LCO interfaces highlight the crucial role of interfacial charge transfer in inducing superconductivity. For example, in LSCO ($x = 0.45$)/LCO heterostructures, superconductivity resides at the second Cu–O plane on the LCO side, whereas a standalone LCO layer is a Mott insulator without mobile charges.[2] Holes in that Cu–O plane are transferred from the LSCO layer, driven by the chemical potential difference between LSCO and LCO. This suggests that interface superconductivity emerges once the LCO layer receives sufficient hole doping through charge transfer. This conjecture is further reinforced by the discovery of superconductivity in the $PrBa_2Cu_3O_7/La_2CuO_4$ interface.[14] It also aligns with the insulating-to-superconducting transition observed in LCO films when holes are introduced by ionic liquid gating.[15]

Following this line of thought, it would be highly intriguing to test whether an undoped cuprate, when placed in proximity to oxides other than cuprates, can give rise to superconductivity. A heterostructure of particular interest is that of a manganite/undoped cuprate, since charges transferred from the manganite layer are spin-polarized when the manganite is chemically doped into a ferromagnetic phase. Whether such spin-polarized charge transfer can induce novel superconductivity—for instance, p-wave pairing—remains an exciting open question.[16–19] This possibility is further motivated by recent discoveries of the coexistence of superconductivity and ferromagnetism at interface superconducting $LaAlO_3/SrTiO_3$,[20–23] $LaAlO_3/KTaO_3$ (111),[9] $YAlO_3/KTaO_3$ (111),[9] and $EuO/KTaO_3$.[11–13]

*Corresponding author. Email: wujie@westlake.edu.cn
© 2026 Chinese Physical Society and IOP Publishing Ltd. All rights, including for text and data mining, AI training, and similar technologies, are reserved.

We selected undoped LCO or SCO as the layer receiving transferred holes or electrons, respectively. SCO is the undoped parent compound of the electron-doped high-temperature superconductor $Sr_{1-x}La_xCuO_2$.[24] The layer serving as the source of holes or electrons is $La_{1-x}Sr_xMnO_3$ (LSMO), which can be tuned by chemical doping from a ferromagnetic metal (for $0.2 < x < 0.5$) to an antiferromagnetic insulator (for $0.5 < x < 1.0$).[25,26] To probe its effect on interface superconductivity, we chose three representative chemical doping levels—$x = 0.33$, 0.67, and 0.8—denoted as LSMO(0.33), LSMO(0.67), and LSMO(0.8), respectively, covering distinct electronic and magnetic states of LSMO. Moreover, it is also interesting to examine whether proximity to a cuprate layer can influence the ferromagnetism of LSMO(0.33).

2. Results and Discussion. Manganite/cuprate heterostructures were grown on $LaSrAlO_4$ (001) (LSAO) substrates by pulsed laser deposition. For control of variables, the thicknesses of the manganite films and cuprate layers were kept at 26 nm and 6.5 nm, respectively, in all samples. For simplicity, we denote, for example, the [26 nm LSMO(0.33)]/[6.5 nm LCO]/[LSAO(001)] heterostructure as LSMO(0.33)/LCO.

X-ray diffraction (XRD) on the LSMO film and heterostructures shows clear diffraction peaks corresponding to the LSMO, LCO, and SCO lattices, confirming that their lattice structures are all single crystalline, consistent with the nature of epitaxial growth [Fig. 1(a)]. The peaks corresponding to LSMO, LCO, and SCO diffraction shift to lower angles relative to their bulk values, indicating an out-of-plane lattice expansion caused by in-plane compressive strain from the LSAO substrate. In addition, the peaks corresponding to LSMO in the heterostructures shift slightly compared to those in the single films, which might be a consequence of the buffer layer LCO or SCO.

Surface morphology of the synthesized films is characterized by atomic-force microscopy (AFM) [Figs. 1(b)–1(d)]. The root-mean-square (RMS) roughness over the measured area of $5 \times 5\,\mu m$ of three representative films yields 0.27 nm, 0.44 nm, and 0.33 nm for LSMO(0.33), LSMO(0.33)/LCO, and LSMO(0.67) films, respectively, indicating atomically flat surfaces, which is crucial for the formation of high-quality interfaces.

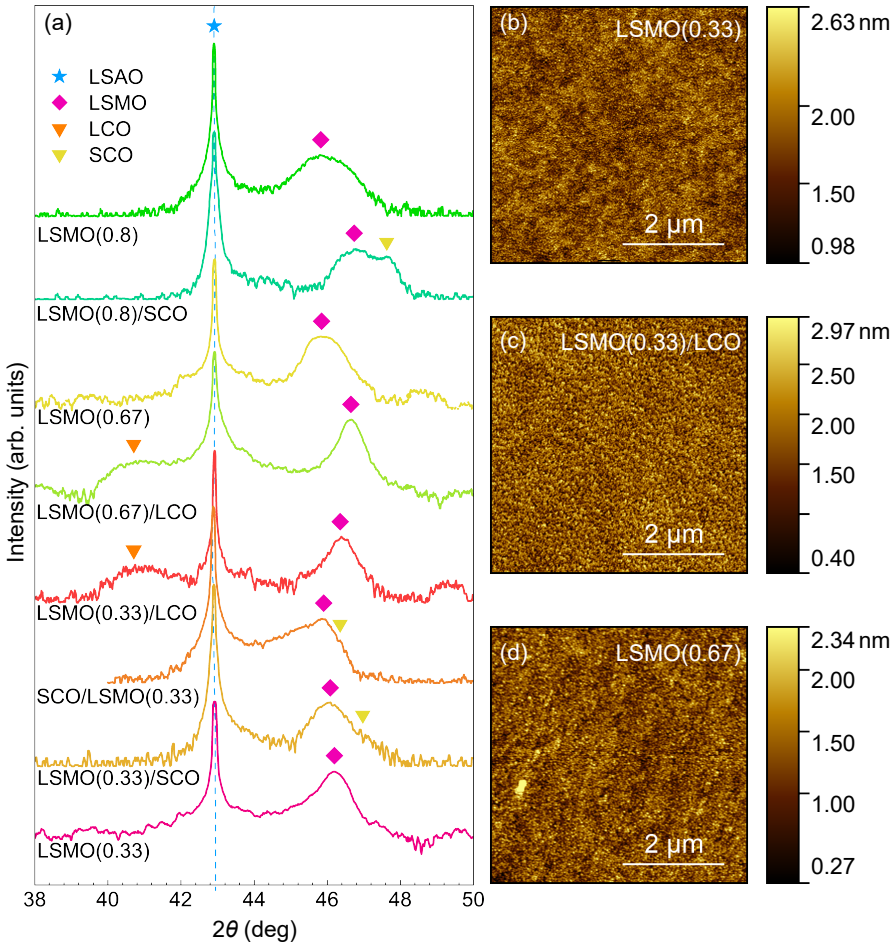

Fig. 1. Structural and morphological characterizations. (a) XRD 2θ–θ scans for the LSMO film and heterostructures grown on LSAO(001) substrates. Symbols mark reflections from the LSAO substrate and film layers (LSMO, LCO, SCO). (b)–(d) AFM topographies of three representative films and heterostructures with sub-nanometer roughness of RMS $\approx$ 0.27 nm, 0.44 nm, and 0.33 nm for LSMO(0.33), LSMO(0.33)/LCO, and LSMO(0.67), respectively (A/B denotes top/bottom stacking). All samples were grown by PLD with nominal thicknesses of 26 nm (LSMO) and 6.5 nm (LCO or SCO).

Table 1. Work functions on LSMO, LCO, and SCO fresh surfaces measured by UPS on various samples and/or various positions.

Material	Φ data points (eV)	Φ (mean ± std) (eV)
LSMO(0.33)	4.62, 4.71	4.67 ± 0.06
SCO	4.46, 4.48, 4.48, 4.7	4.53 ± 0.11
LCO	4.26, 4.46, 4.56, 4.6	4.47 ± 0.15

Interfacial charge transfer is driven by the difference in work functions of two proximate compounds.[27] To determine the direction of charge flow across the interface, we measured the surface work functions Φ of LSMO, SCO, and LCO using ultraviolet photoemission spectroscopy (UPS). After deposition, LSMO, SCO, or LCO films were transferred from the pulsed laser deposition (PLD) growth chamber to the UPS chamber without breaking the vacuum, thus avoiding contamination caused by exposure to air and thereby promoting the integrity and reliability of the acquired work function data. Prior to measurements of each batch of samples, a gold reference film was freshly deposited on the substrate in an ion sputtering coating instrument and transferred through the atmosphere into the UPS chamber immediately.

Multiple work function measurements were performed on various samples and/or various positions, yielding statistical data on the work functions of surfaces with different compositions, as presented in Table 1. For LSMO(0.33), SCO, and LCO, the work functions are 4.67 ± 0.06, 4.53 ± 0.11, and 4.47 ± 0.15 eV, respectively. We notice that the work function of samples with identical composition can vary within a range of approximately ± 0.1 eV due to the high sensitivity of the work function to surface termination and contamination.[28] Nevertheless, the observed inter-group difference is statistically significant compared to the intra-group variation, allowing us to conclude that $\Phi_{\mathrm{LSMO}(0.33)} > \Phi_{\mathrm{SCO}} > \Phi_{\mathrm{LCO}}$. Although work functions of LSMO(0.67) and LSMO(0.8) thin films were not measured in this work, it has been reported[29] that LSMO exhibits a decreasing chemical potential as x increases; hence, $\Phi_{\mathrm{LSMO}(0.8)} > \Phi_{\mathrm{LSMO}(0.67)} > \Phi_{\mathrm{LSMO}(0.33)} > \Phi_{\mathrm{SCO}} > \Phi_{\mathrm{LCO}}$. As a result, electrons are expected to transfer from the cuprate with the lower work function into the LSMO with the higher work function until the electrochemical potentials equalize, leaving holes accumulated on the cuprate side. Notably, while $\Phi_{\mathrm{LSMO}(0.33)}$ is consistent with prior reports,[30–32] Φ_{LCO} here is lower than previously reported.[33]

Electric transport of LSMO films and heterostructures were carried out on Hall bars patterned by standard UV lithography and lift-off techniques. The LSMO(0.33) film is metallic over the full temperature range of 1.8–320 K, while the LSMO(0.67) and LSMO(0.8) films are both insulating (Fig. 2), consistent with previous reports.[25,34] This confirms the quality of the LSMO films we synthesized.

The SCO/LSMO(0.33), LSMO(0.33)/SCO, and LSMO(0.33)/LCO heterostructures remain metallic down to 1.8 K, the lowest temperature accessible to us, without any discernible resistive drop associated with a superconducting transition [Fig. 2(a)]. Relative to the LSMO(0.33) film, the heterostructures show increased resistance. At first glance, this appears inconsistent with the expectation that holes are transferred into the undoped cuprate layer due to the work-function hierarchy, which should enhance its conductivity. This apparent discrepancy can be understood by considering two competing effects. In the LSMO(0.33) layer, hole depletion reduces its carrier density and therefore its conductivity. Meanwhile, the amount of holes transferred into the LCO or SCO layer is insufficient to drive the insulating cuprate metallic. Consequently, any conductivity gain in the cuprate layer cannot offset the conductivity loss in the LSMO layer, resulting in an overall increase in resistance.

To assess the influence of epitaxial strain, we reversed the stacking order of the SCO and LSMO(0.33) layers. From the XRD measurements (Fig. 1), the LSMO peak positions remain nearly identical for both SCO/LSMO(0.33) and LSMO(0.33)/SCO, whereas the SCO peaks shift to lower angles in SCO/LSMO(0.33) than in LSMO(0.33)/SCO. This indicates a larger c-axis lattice constant for SCO when grown atop LSMO(0.33), consistent with strain relaxation as film thickness increases. As a result, the SCO layer experiences weaker (stronger) epitaxial strain when positioned above (below) the LSMO

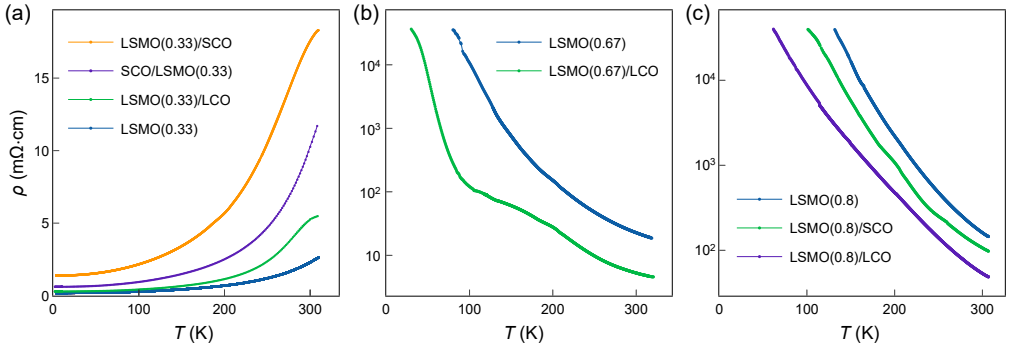

Fig. 2. Temperature-dependent resistivity, $\rho(T)$, for LSMO films and heterostructures. (a) $\rho(T)$ for the metallic LSMO(0.33) film and its heterostructures with LCO and SCO. (b) and (c) $\rho(T)$ for the insulating LSMO and its heterostructure with LCO and SCO for LSMO(0.67) and LSMO(0.8), respectively. No signature of interface superconductivity is present down to 1.8 K in any of the above samples.

layer. Correspondingly, the SCO/LSMO(0.33) heterostructures (with LSMO at the bottom) exhibit a resistivity reduced to ∼64% of that of LSMO(0.33)/SCO at 320 K. Despite these strain-induced structural and transport differences, neither heterostructure shows any indication of superconductivity down to 1.8 K.

To further strengthen the interfacial charge transfer, we replaced the LSMO(0.33) layer with LSMO(0.67) and LSMO(0.8). Because the work functions follow the relation $\Phi_{\mathrm{LSMO(0.8)}} > \Phi_{\mathrm{LSMO(0.67)}} > \Phi_{\mathrm{LSMO(0.33)}} > \Phi_{\mathrm{SCO}} > \Phi_{\mathrm{LCO}}$, the work-function difference between LSMO and SCO or LCO increases as the chemical doping level of LSMO increases, thereby driving more charge transfer across the interface. The SCO and LCO films are too insulating to be measured using our transport setup. However, when interfaced with LCO, the LSMO(0.67) layer manifests a resistivity almost an order of magnitude lower than that of the LSMO(0.67) film [Fig. 2(b)]. A similar trend is observed for higher-doped LSMO: the resistivities of LSMO(0.8)/SCO and LSMO(0.8)/LCO decrease by approximately factors of 3 and 9, respectively, relative to the LSMO(0.8) film [Fig. 2(c)].

Such a substantial enhancement in conductivity in the heterostructures can only be explained by the formation of a conducting layer at the LSMO/SCO and LSMO/LCO interfaces. However, it is somewhat disappointing that this conducting layer does not enter the superconducting state at low temperatures, unlike the interface-superconducting LSCO/LCO heterostructures.

LSMO(0.33) is a ferromagnetic metal, while LCO and SCO are both antiferromagnetic Mott insulators. The proximity effect of the LCO or SCO layer on the ferromagnetism of LSMO was investigated through magneto-transport measurements. After subtracting the contributions from contact misalignment and separating contributions from both the ordinary and anomalous Hall effects (AHE) (with the data-processing procedure detailed in the Methods section), the AHE resistivity $\rho_{xy}^{\mathrm{AHE}}(H)$ for the LSMO(0.33) film clearly manifests hysteresis behavior [Fig. 3(a)]. Consistent with previous findings, the ordinary Hall coefficient R_{H} changes sign as the temperature increases,[35–39] indicating temperature-dependent contributions from both hole and electron pockets at the Fermi surface.[40] The AHE originates from the ferromagnetism of LSMO(0.33), which diminishes at its Curie temperature (T_{C}) of approximately 320 K. The hysteresis loops associated with the AHE vary noticeably in shape with temperature, plausibly reflecting the complex magnetization dynamics under the influence of the external magnetic field, magnetic anisotropy, and the demagnetization field. In addition, the magnetic anisotropy of LSMO(0.33) is sensitive to epitaxial strain, disorder, and growth conditions, and may undergo a spin reorientation transition between in-plane and out-of-plane directions as the temperature changes.[25,41] For the LSMO(0.33)/SCO [Fig. 3(b)], SCO/LSMO(0.33) [Fig. 3(c)], and LSMO(0.33)/LCO [Fig. 3(d)] heterostructures, the AHE hysteresis loops differ noticeably from those of the LSMO films, indicating that the magnetization dynamics are significantly influenced by the adjacent SCO or LCO layer. The interfacial coupling between the antiferromagnetic cuprate layer and the ferromagnetic LSMO layer introduces additional pinning of the LSMO magnetization, thereby modifying the coercivity and domain-wall motion dynamics.

Generally speaking, the carrier density in a material can be estimated using the Drude formula $n = 1/(eR_{\mathrm{H}})$, where R_{H} is the Hall coefficient of the ordinary Hall effect. However, this simple interpretation is not applicable to LSMO films. In LSMO, multiple bands cross the Fermi level, giving rise to both electron- and hole-like pockets, and the resulting Hall coefficient is strongly temperature

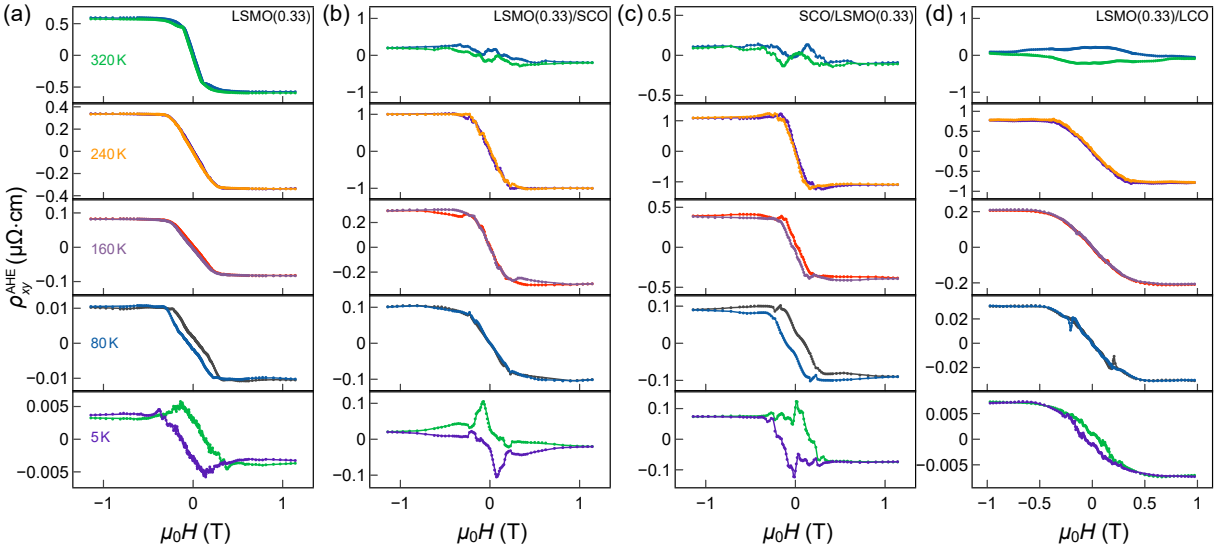

Fig. 3. Anomalous Hall effect in the LSMO(0.33) film and its heterostructures. The AHE resistivity, $\rho_{xy}^{\mathrm{AHE}}(\mu_0 H)$, was measured for (a) the LSMO(0.33) film, (b) LSMO(0.33)/SCO, (c) SCO/LSMO(0.33), and (d) LSMO(0.33)/LCO heterostructures at $T = 320$, 240, 160, 80, and 5 K (from top to bottom).

dependent and even exhibits sign reversal.[35–40] Moreover, in LSMO-based heterostructures, both the LSMO layer and the adjacent cuprate layer (LCO or SCO) contribute to the Hall response, while possessing distinct carrier densities and mobilities. This further complicates a straightforward interpretation of the Hall coefficient. Nevertheless, since the undoped LCO or SCO layer is insulating, the Hall coefficient would remain unchanged between the bare LSMO film and the heterostructure in the absence of interfacial charge transfer. Therefore, although $n_{\text{eff}} \equiv 1/(eR_{\text{H}})$ cannot be directly interpreted as the true carrier density, variations in n_{eff} can still serve as a qualitative indicator of interfacial charge transfer.

As shown in Table 2, interfacing LSMO(0.33) with either LCO or SCO cuprate films leads to a decreased n_{eff} compared to the LSMO film. This trend indicates charge transfer—likely hole depletion from the LSMO layer—consistent with the work-function data. For the higher doping levels in Table 3, LSMO(0.67) and LSMO(0.8) also exhibit a decreased n_{eff} when interfaced with LCO. However, a distinct increase in n_{eff} is observed for LSMO(0.8) when interfaced with SCO, which could stem from an interface-induced modification of the electron–hole compensation, considering the multiband nature. Therefore, the changes in Hall coefficients evidence substantial charge transfer across the LSMO–cuprate interface.

The absence of interface superconductivity in manganite/cuprate heterostructures is unexpected given the prevailing picture that interfacial charge transfer into an undoped cuprate layer should induce high-temperature superconductivity, as observed in interface-superconducting LSCO/LCO and $PrBa_2Cu_3O_7/La_2CuO_4$ heterostructures. One possibility is that the transferred charge might not be sufficient to dope the cuprate layer across the insulator-to-superconductor transition. From the work-function measurements (Table 1), the difference between the cuprates and LSMO(0.33) is within approximately 0.2 eV, and this difference increases further for the heavily doped LSMO(0.67) and LSMO(0.8)—for comparison, the work-function difference between LSCO(0.45) and LCO is ∼0.3 eV. Thus, an estimation based on layer-dependent Poisson equation predicts that the LCO layer nearest to and second-nearest to the interface receives sufficient holes to fall within the superconducting dome,[3,42,43] thereby ruling out charge insufficiency as a primary cause.

Table 2. The ordinary Hall coefficient R_{H} and $n_{\text{eff}} = 1/(eR_{\text{H}})$ of the LSMO(0.33) film and heterostructures measured at 80 K.

Sample	R_{H} (m^3/C)	n_{eff} (cm^{-3})
LSMO(0.33)	0.03058	2.041×10^{22}
LSMO(0.33)/LCO	0.03862	1.616×10^{22}
LSMO(0.33)/SCO	0.12427	5.022×10^{21}
SCO/LSMO(0.33)	0.04556	1.370×10^{22}

Table 3. R_{H} and n_{eff} of the LSMO(0.67) and LSMO(0.8) films and heterostructures measured at 250 K.

Sample	R_{H} (m^3/C)	n_{eff} (cm^{-3})
LSMO(0.67)	−1.7129	-3.644×10^{20}
LSMO(0.67)/LCO	−0.08196	-7.615×10^{21}
LSMO(0.8)	−1.29721	-4.811×10^{20}
LSMO(0.8)/LCO	−0.36139	-1.727×10^{21}
LSMO(0.8)/SCO	0.09441	6.611×10^{21}

Contrasting the LSCO/LCO and LSMO(0.33)/LCO heterostructures, one major difference is that the charge transferred from LSMO(0.33) is spin-polarized due to its ferromagnetism, which is unfavorable for superconductivity since Cooper pairs are formed by two electrons with opposite spins. However, in the antiferromagnetic LSMO(0.67) and LSMO(0.8), the transferred charges are not spin-polarized, yet neither the LSMO(0.67)/cuprate nor the LSMO(0.8)/cuprate heterostructures show superconductivity. This observation suggests that spin-polarized charge transfer alone cannot account for the absence of superconductivity.

Due to quantum tunneling, quantum order extends across the interface and gives rise to the proximity effect.[27] The ferromagnetic or antiferromagnetic order parameter is induced in the undoped cuprate layer by the adjacent LSMO layer, leading to a competition between superconductivity and magnetism for the ground state. This competition might effectively suppress the emergence of superconductivity. This interpretation is consistent with the AHE analysis in Fig. 3, which reveals modified hysteresis behavior arising from interfacial coupling between the antiferromagnetism in the undoped cuprate and the ferromagnetism in the LSMO(0.33) layer.

3. Conclusion. We conducted a systematic investigation of high-quality heterostructures consisting of LSMO and LCO or SCO to search for interface superconductivity. The UPS measurements confirm that there is an appreciable difference in work function sufficient to drive interfacial charge transfer. Increasing the chemical doping in the LSMO layer from 0.33 to 0.80 evolves LSMO from a ferromagnetic metal to an antiferromagnetic insulator. These manganite/cuprate heterostructures accommodate an interfacial conducting layer. The absence of superconductivity is likely attributable to spin-polarized charge transfer and the competition between superconductivity and magnetism. Our findings provide valuable insights into the rapidly expanding field of interface superconductivity and guide the exploration of emergent interfacial quantum phases.

4. Methods.

4.1. Film Growth, Structural Characterizations and Device Fabrication. Films were grown on $LaSrAlO_4$ (001) single-crystal substrates by pulsed laser deposition (PLD). The laser fluence and repetition rate were 1.8 $\text{J}\cdot\text{cm}^{-2}$ and 2 Hz, respectively. LSMO layers were deposited at a substrate temperature of 640 ℃ and an O_2 partial pressure of 7×10^{-2} mbar. For cuprate layers, LCO and SCO were deposited at substrate temperatures of 675 ℃ and 550 ℃, respectively, under an O_2 partial pressure of 8.5×10^{-2} mbar. Film thickness was monitored and controlled by reflection high-energy electron diffraction (RHEED) intensity oscillations and pre-calibrated pulse counts.

For structural characterization, a high-resolution thin-film X-ray diffractometer (HRXRD, Bruker D8 Discover,

Cu K_α radiation, $\lambda = 1.5406\,\text{Å}$) was used. The surface morphology of the films was imaged in tapping mode using atomic force microscopy (AFM, BenYuan BY2000).

Hall-bar devices of 300 µm width were patterned using standard optical lithography and ion-milling techniques. To form Ohmic contacts, 50 nm of Au was deposited onto the contact pads using an automated sputter coater (EMS 150TS).

4.2. Ultraviolet Photoelectron Spectroscopy (UPS). Work functions of thin films were measured using the Thermo Fisher ESCALAB Xi+ UPS system with He I radiation (21.22 eV). The UPS chamber is connected to the PLD chamber, enabling sample transfer without breaking vacuum. Prior to film deposition, silver paint was applied to the edge of the substrate's top surface and connected to the sample holder, establishing reliable electrical grounding. Right after film deposition, the films were transferred immediately from the PLD chamber to the UPS chamber for work-function measurement, preventing surface contamination. 20 nm-thick gold films were coated on LSAO substrates as a reference to calibrate the Fermi level.

4.3. Electrical Transport Measurements. Electrical transport measurements were performed on a DynaCool Physical Property Measurement System (Quantum Design, PPMS).

Due to the inevitable contact misalignment, the longitudinal resistivity, $\rho_{xx}(H)$, is unavoidably superposed on the measured transverse resistivity, $\rho_{xy}(H)$. This spurious contribution can be eliminated by reversing the magnetic field direction. In principle, $\rho_{xy}^{\text{Hall}}(H)$—the sum of the ordinary Hall and anomalous Hall contributions—should change sign while maintaining its amplitude upon field reversal when the magnetic field is larger than the coercivity of the AHE. In contrast, $\rho_{xy}^{\text{MR}}(H)$, arising from contact misalignment and therefore proportional to $\rho_{xx}(H)$, remains unchanged when the field direction is reversed. Accordingly, $\rho_{xy}(H)$ is obtained by subtracting $\rho_{xx}(H)$ and an offset constant b,

$$\rho_{xy}^{\text{Hall}}(H) = \rho_{xy}(H) - a\,\rho_{xx}(H) - b.$$

When the magnetic field exceeds the coercive field of the ferromagnetic LSMO(0.33), $\rho_{xy}(H)$ exhibits a linear dependence on H. Moreover, the slopes for the positive and negative high-field regions become identical. This constraint enables the determination of the coefficient a in the expression above.

Next, $\rho_{xy}^{\text{Hall}}(H)$ can be further separated into two contributions: $\rho_{xy}^{\text{Hall}}(H) = \rho_{xy}^{\text{OHE}}(H) + \rho_{xy}^{\text{AHE}}(H)$. Here, $\rho_{xy}^{\text{OHE}}(H)$ and $\rho_{xy}^{\text{AHE}}(H)$ are the ordinary Hall and anomalous Hall resistivities, respectively. For magnetic fields larger than the coercive field, $\rho_{xy}^{\text{AHE}}(H)$ is saturated and becomes field independent, so the slope of $\rho_{xy}^{\text{Hall}}(H)$ comes entirely from $\rho_{xy}^{\text{OHE}}(H)$. From the best linear fitting, we can extract this slope k, and then we have the relation $\rho_{xy}^{\text{OHE}}(H) = k\,H$ for all magnetic fields. By subtracting $\rho_{xy}^{\text{OHE}}(H)$ from $\rho_{xy}^{\text{Hall}}(H)$, we obtain $\rho_{xy}^{\text{AHE}}(H)$.

Data Availability. The data that support the findings of this study and all other relevant data are available from the corresponding author upon request.

Acknowledgements. This work was supported by the National Key R&D Program of China (Grant Nos. 2023YFA1406400 and 2024YFA1408102), Research Center for Industries of the Future at Westlake University (Project No. WU2023C001), the National Natural Science Foundation of China (Grant No. 12174318), and the Zhejiang Provincial Natural Science Foundation of China (Grant No. XHD23A2002). We acknowledge the assistance provided by the Instrumentation and Service Center for Physical Sciences and for Molecular Science at Westlake University.

References

[1] Gozar A, Logvenov G, Kourkoutis L F, Bollinger A T, Giannuzzi L A, Muller D A, and Bozovic I 2008 *Nature* **455** 782
[2] Logvenov G, Gozar A, and Bozovic I 2009 *Science* **326** 699
[3] Wu J, Pelleg O, Logvenov G, Bollinger A T, Sun Y J, Boebinger G S, Vanević M, Radović Z, and Božović I 2013 *Nat. Mater.* **12** 877
[4] Shi C Y, Ju L L, Wang Y Z, Zhang M, Sun J R, and Xie Y W 2025 *Phys. Rev. B* **112** 174505
[5] Wang Q Y, Li Z, Zhang W H, Zhang Z C, Zhang J S, Li W, Ding H, Ou Y B, Deng P, Chang K, Wen J, Song C L, He K, Jia J F, Ji S H, Wang Y Y, Wang L L, Chen X, Ma X C, and Xue Q K 2012 *Chin. Phys. Lett.* **29** 037402
[6] Ding H, Lv Y F, Zhao K, Wang W L, Wang L L, Song C L, Chen X, Ma X C, and Xue Q K 2016 *Phys. Rev. Lett.* **117** 67001
[7] Zhou G Y, Zhang Q H, Zheng F W, Zhang D, Liu C, Wang X X, Song C L, He K, Ma X C, Gu L, Zhang P, Wang L L, and Xue Q K 2018 *Sci. Bull.* **63** 747
[8] Reyren N, Thiel S, Caviglia A D, Kourkoutis L F, Hammerl G, Richter C, Schneider C W, Kopp T, Rüetschi A S, Jaccard D, Gabay M, Muller D A, Triscone J M, and Mannhart J 2007 *Science* **317** 1196
[9] Ning Z F, Qian J H, Liu Y X, Chen F, Zhang M Z, Deng L W, Yuan X, Ge Q Q, Jin H, Zhang G Q, Peng W, Qiao S, Mu G, Chen Y, and Li W 2024 *Nano Lett.* **24** 7134
[10] Chen Z, Liu Z R, Sun Y Q, Chen X X, Liu Y, Zhang H, Li H K, Zhang M, Hong S Y, Ren T S, Zhang C, Tian H, Zhou Y, Sun J R, and Xie Y W 2021 *Phys. Rev. Lett.* **126** 26802
[11] Liu C, Yan X, Jin D F, Ma Y, Hsiao H W, Lin Y L, Bretz-Sullivan T M, Zhou X, Pearson J, Fisher B, Jiang J S, Han W, Zuo J M, Wen J G, Fong D D, Sun J R, Zhou H, and Bhattacharya A 2021 *Science* **371** 716
[12] Hua X Y, Meng F B, Huang Z Y, Li Z H, Wang S, Ge B, Xiang Z J, and Chen X H 2022 *npj Quantum Mater.* **7** 97
[13] Hua X Y, Zeng Z M, Meng F B, Yao H X, Huang Z Y, Long X Y, Li Z H, Wang Y F, Wang Z Y, Wu T, Weng Z Y, Wang Y H, Liu Z, Xiang Z J, and Chen X H 2024 *Nat. Phys.* **20** 957
[14] Ju L L, Ren T S, Shi C Y, and Xie Y W 2022 *J. Appl. Phys.* **132** 225306
[15] Garcia-Barriocanal J, Kobrinskii A, Leng X, Kinney J, Yang B, Snyder S, and Goldman A M 2013 *Phys. Rev. B* **87** 024509
[16] Read N and Green D 2000 *Phys. Rev. B* **61** 10267
[17] Santos L, Neupert T, Chamon C, and Mudry C 2010 *Phys. Rev. B* **81** 184502

[18] Ran S, Eckberg C, Ding Q P, Furukawa Y, Metz T, Saha S R, Liu I L, Zic M, Kim H, Paglione J, and Butch N P 2019 *Science* **365** 684
[19] Cao Z K, Li J Y, Su J H, Ying T, and Tang H K 2025 *Phys. Rev. B* **111** 24509
[20] Mehta M, Dikin D A, Bark C W, Folkman C M, Eom C B, and Chandrasekhar V 2012 *J. Phys. Conf. Ser.* **400** 022071
[21] Li L, Richter C, Mannhart J, and Ashoori R C 2011 *Nat. Phys.* **7** 762
[22] Bert J A, Kalisky B, Bell C, Kim M, Hikita Y, Hwang H Y, and Moler K A 2011 *Nat. Phys.* **7** 767
[23] Dikin D A, Mehta M, Bark C W, Folkman C M, Eom C B, and Chandrasekhar V 2011 *Phys. Rev. Lett.* **107** 056802
[24] Kikkawa S, Er G, and Kanamaru F 1993 *Appl. Supercond.* **1** 487
[25] Hemberger J, Krimmel A, Kurz T, Krug von Nidda H A, Ivanov V Yu, Mukhin A A, Balbashov A M, and Loidl A 2002 *Phys. Rev. B* **66** 094410
[26] Dagotto E, Hotta T and Moreo A 2001 *Phys. Rep.* **344** 1
[27] Kivelson S A 2002 *Physica B* **318** 61
[28] Minohara M, Yasuhara R, Kumigashira H, and Oshima M 2010 *Phys. Rev. B* **81** 235322
[29] Matsuno J, Fujimori A, Takeda Y, and Takano M 2002 *Europhys. Lett.* **59** 252
[30] de Jong M P, Dediu V A, Taliani C, and Salaneck W R 2003 *J. Appl. Phys.* **94** 7292
[31] Reagor D W, Lee S Y, Li Y, and Jia Q X 2004 *J. Appl. Phys.* **95** 7971
[32] Minohara M, Ohkubo I, Kumigashira H, and Oshima M 2007 *Appl. Phys. Lett.* **90** 132123
[33] Yunoki S, Moreo A, Dagotto E, Okamoto S, Kancharla S S, and Fujimori A 2007 *Phys. Rev. B* **76** 064532
[34] Urushibara A, Moritomo Y, Arima T, Asamitsu A, Kido G, and Tokura Y 1995 *Phys. Rev. B* **51** 14103
[35] Dildar I M, Beekman C, He X, and Aarts J 2012 *Phys. Rev. B* **85** 205103
[36] Lyanda-Geller Y, Chun S H, Salamon M B, Goldbart P M, Han P D, Tomioka Y, Asamitsu A, and Tokura Y 2001 *Phys. Rev. B* **63** 184426
[37] Asamitsu A and Tokura Y 1998 *Phys. Rev. B* **58** 47
[38] Mashkautsan V V, Zainullina R I, Bebenin N G, Ustinov V V, and Mukovskii Ya M 2003 *Phys. Solid State* **45** 494
[39] Matl P, Ong N P, Yan Y F, Li Y Q, Studebaker D, Baum T, and Doubinina G 1998 *Phys. Rev. B* **57** 10248
[40] Shi M, Falub M C, Willmott P R, Krempasky J, Herger R, Patthey L, Hricovini K, Falub C V, and Schneider M 2008 *J. Phys.: Condens. Matter* **20** 222001
[41] Liao Z L and Zhang J D 2019 *Appl. Sci.* **9** 144
[42] Loktev V M and Pogorelov Yu G 2008 *Phys. Rev. B* **78** 180501
[43] Radović Z, Vanević M, Wu J, Bollinger A T, and Božović I 2017 *J. Supercond. Novel Magn.* **30** 725